REPORT DOCUMENTATION PAGE

Form Approved
OMB No. 0704-0188

1. REPORT DATE *(DD-MM-YYYY)*	2. REPORT TYPE	3. DATES COVERED *(From - To)*
04 02-2008	Journal Article	28 Jan 08 – 04-Feb-2008

4. TITLE AND SUBTITLE

A-law/μ-law Dynamic Range Compression Deconvolution (Pre-Print)

5a. CONTRACT NUMBER
IN-HOUSE

5b. GRANT NUMBER

5c. PROGRAM ELEMENT NUMBER
61102F

6. AUTHOR(S)

*Bahareh Haji-saeed, *John Kierstead, **William D. Goodhue, Jed Khoury, Charles L. Woods

5d. PROJECT NUMBER
2305

5e. TASK NUMBER
HC

5f. WORK UNIT NUMBER
01

7. PERFORMING ORGANIZATION NAME(S) AND ADDRESS(ES)
AND ADDRESS(ES)
Optoelectronic Technology Branch (AFRL/RYHC), 80 Scott Drive, Hanscom AFB, MA 01731, 2909; *Solid State Scientific Corporation, Hollis, NH 03049; **University of MASS, Lowell, MA, 01854;

8. PERFORMING ORGANIZATION REPORT

9. SPONSORING / MONITORING AGENCY NAME(S) AND ADDRESS(ES)
Electromagnetics Technology Division Source Code: 437890
Sensors Directorate
Air Force Research Laboratory
80 Scott Drive
Hanscom AFB MA 01731-2909

10. SPONSOR/MONITOR'S ACRONYM(S)
AFRL-RY-HS

11. SPONSOR/MONITOR'S REPORT NUMBER(S)
AFRL-RY-HS-TP-2008-0025

12. DISTRIBUTION / AVAILABILITY STATEMENT
DISTRIBUTION A: APPROVED FOR PUBLIC RELEASE: DISTRIBUTION UNLIMITED.

13. SUPPLEMENTARY NOTES
Submitted to Applied Optics, for publication. Not to be released for pre-publication. The U.S. Government is joint author of this work and has the right to use, modify, reproduce, release, perform, display, or disclose the work. Cleared for Public Release by ESC/PA number: ESC-08-0135.

14. ABSTRACT
In this paper the A-law/μ-law Dynamic Range Compression algorithm used in telecommunication systems is proposed for the first time for nonlinear Dynamic Range Compression image restoration of blurred signals embedded in very high noise environment. Our simulation results demonstrate that the dynamic range compression image deconvolution via the A-law/μ-law outperforms image restoration based on the well-established image restoration filters that have been used for the last fifty year such as Wiener filter and Inverse filter. The deconvolution orders have been analyzed using the nonlinear transform method.

15. SUBJECT TERMS
adaptive optics, deconvolution, nonlinear image processing

16. SECURITY CLASSIFICATION OF:			17.LIMITATION OF ABSTRACT	18.NUMBER OF PAGES	19a. NAME OF RESPONSIBLE PERSON
a. REPORT	b. ABSTRACT	c. THIS PAGE			Jed Khoury
Unclassified	Unclassified	Unclassified	SAR	39	19b. TELEPHONE NUMBER *(include area code)* N/A

Standard Form 298 (Rev. 8-98)
Prescribed by ANSI Std. Z39.18

A-law/μ-law Dynamic Range Compression Deconvolution

Bahareh Haji-saeed[1], Jed Khoury[2], William D. Goodhue[3], Charles L. Woods[2], and John Kierstead[1]

[1]*Solid State Scientific Corporation, Hollis, NH 03049*
[2]*Air Force Research Laboratory / RYHC, Hanscom Air Force Base, MA 01731*
[3]*Physics Department, University of Massachusetts Lowell, Lowell, Massachusetts 01854*

Abstract: In this paper the A-law/μ-law Dynamic Range Compression algorithm used in telecommunication systems is proposed for the first time for nonlinear Dynamic Range Compression image restoration of blurred signals embedded in very high noise environment. Our simulation results demonstrate that the dynamic range compression image deconvolution via the A-law/μ-law outperforms image restoration based on the well-established image restoration filters that have been used for the last fifty year such as Wiener filter and Inverse filter. The deconvolution orders have been analyzed using the nonlinear transform method.

Keywords: adaptive optics, deconvolution, nonlinear image processing

Introduction

Dynamic Range Compression/Expansion known as companding (compressing-expanding) is a well-established principle for recovering the signal embedded in high noise. Dynamic Range Compression accompanied with conventional image restoration might be useful in recovering images embedded in a high noise environment. Dynamic Range Compression/Expansion nonlinearity, when applied to a noisy signal, improves the signal to noise ratio in areas where the signal is low compared to the noise and reduces the SNR in areas where the signal is higher than the noise level. This principle has been used for improving the quality of acoustic signals in the 50's and is extensively used for noise reduction in tape recording which is limited by "tape hiss", which is high frequency random noise. Noise reduction systems like the "Dolby" and "dbx" help to solve this problem by pre-emphasizing (compression) the high frequencies before recording onto tape in order to make them higher in amplitude than the tape hiss noise with which they compete and then upon playback, a matched de-emphasis filter (expansion) is employed. These noise reduction systems are amplitude sensitive so that only soft high-frequency sounds are emphasized. And the matched de-emphasis filter scales the high frequencies to their right position with the other recorded signals[1].

Dynamic Range Compression/Expansion technique has also been used in telecommunication systems using a nonlinear element for simultaneously compressing the data (reducing the signal's dynamic range for uniform quantization process), enhancing the SNR and at the receiver end expanding the data through the inverse of the same nonlinear element [2,3].

The use of Dynamic Range Compression techniques and power-law nonlinear transfer functions are not new for image processing purposes. Techniques such as contrast stretching[4] which

compress the data (by a nonlinear transfer function) below a threshold value to darken the image for higher contrast, image enhancement using gray-level nonlinear transformation functions (like logarithmic transformation[4-6] and power-law transformation[4]) and simultaneous gray-level compression and contrast enhancement or multiplicative to additive noise conversion using homomorphic nonlinear filtering has been examined[4,6].

In this paper, Dynamic Range Compression image deconvolution via both the A-law and the μ-law encoders is introduced for the first time. In image deconvolution of a noisy and blurred signal, dynamic range compression performs the following dual functions: (1) Enhances the high frequencies of the degraded signal relative to the low frequencies, reducing the blur; (2) Enhances the signal-to-noise ratio in particular at high frequencies even where the signal-to-noise ratio is very low, further improving the finer details in the image. Such an approach overcomes even the optimal Wiener filter[4] limitations. These limitations are described in the next section. Several forms of distortion functions with tested input images are studied and simulated. The distortion functions such as motion distortion, atmospheric turbulence and misfocusing aberration is examined. A human face (Lena) is utilized as an input image. The joint spectra orders for this deconvolution technique are analyzed using the nonlinear transform method[3]: both A-law and the μ-law nonlinear functions are firstly expanded to their power-law nonlinear saturation functions, then the contribution of each order has been calculated and finally all the orders contributions have been combined.

Inverse and Wiener Filters

Inverse filtering[4] is the simplest linear approach for restoring the distorted image. One can compute the estimated restored image by dividing the Fourier transform of the degraded image

$$\hat{F}(u,v) = \frac{G(u,v)}{H(u,v)} = F(u,v) + \frac{N(u,v)}{H(u,v)} \qquad (1)$$

G(u, v) by the Fourier transform of the aberration function *H(u, v)* as stated in the following equation:

Where G(u, v) is the Fourier transform of the distorted image plus noise,

$$G(u,v) = F(u,v)H(u,v) + N(u,v) \qquad (2)$$

Equation 1 tells us that even if the distortion function is known, the undegraded image can not be recovered because of having noise *N(u, v)* in the image. Because the noise is random and the Fourier transform of a random function is random and unknown, therefore *N (u, v)/H (u, v)* ratio could easily dominate the estimated recovered image $\hat{F}(u,v)$ and create a noisy undegraded image and if the noise level is high the recovered image may not be visible. The Inverse filter, for most of blur functions, is a highpass filter and because noise spreads over a broad-band of frequencies therefore after Inverse filtering the noise will be enhanced in high frequencies. To overcome this problem the Wiener filtering method comes into the consideration. This nonlinear approach incorporates both the degradation function and the statistical characteristics of noise into the restoration process. This method considers images and noise as random processes. The

$$W(u,v) = \left[\frac{|H(u,v)|^2 |F(u,v)|^2}{|H(u,v)|^2 |F(u,v)|^2 + |N(u,v)|^2}\right] \times \left[\frac{1}{H(u,v)}\right] \qquad (3)$$

Wiener filter expression could be shown as[7]

where *H(u ,v)* is the distortion function, *H*(u, v)* is the complex conjugate of *H(u, v)*, $|H(u, v)|^2$, $|F(u, v)|^2$ and $|N(u, v)|^2$ are the power spectrum of the distortion function, the undegraded image and the noise respectively.

Accordingly, the Wiener Filter consists of two filters: (a) the proportionality filter (the first term), (b) the inverse filter (the second term). The inverse filter, as it was discussed before, is the best filter for image restoration in a non-noisy environment. The proportionality filter represents

the ratio of the clean blur signal power spectrum to the total power spectrum. For a non-noisy environment, the proportionality filter has 100% transmitivity of the input signal, while in a very high noise this filter transmits nearly 0% of the input signal. Therefore the process behind the Wiener filter consists of two stages: first the noise filtering via the spectrum proportionality filter, and second the signal deblurring via the inverse filter. In this process for regions when SNR is low, the signal in this part of the spectrum will be lost. Therefore, the Wiener filter is not effective in harsh operating conditions such as imaging on a rainy day or in a sandstorm. When the noise is much higher than the signal across the full spectrum, both the noise and the signal are removed. However, our proposed dynamic range compression deconvolution is a new signal recovery technique that can retrieve the signal in a high noise environment while outperforming both inverse and Wiener filters.

Architecture

The architecture of image compression nonlinear joint Fourier processor via A-law/μ-law is shown in Figure 1. This figure shows a joint Fourier processor setup which uses a single input plane for both the reference (r) and the signal (s) images and jointly Fourier transforms the input via a lens. The joint Fourier spectrum then is captured by a CCD camera which acts as a square-law receiver and is responsible for mixing the spectra to produce the cross products. The output from the CCD camera is sent to the A-law/μ-law digital or analog receiver. After nonlinear A-law or μ-law Dynamic Range compression deconvolution the output is sent to a spatial light modulator (SLM), the output from SLM is then Fourier transformed via a lens to produce the processed output. As shown explicitly in the theoretical section, the CCD camera is responsible for combining the Fourier transforms of the impulse response and the distorted image to compensate for the phase distortion. And then the A-law/μ-law nonlinear transformation is

responsible for enhancing high frequencies, and hence noise reduction and signal to noise ratio enhancement. The input-output nonlinear transfer functions of the A-law and the μ-law receivers are respectively defined as[2]

$$f(E) = \frac{1 + \ln A \mid E \mid}{1 + \ln A} \operatorname{sgn}(E) \tag{1}$$

$$f(E) = \frac{\ln(1 + \mu \mid E \mid)}{\ln(1 + \mu)} \operatorname{sgn}(E) \tag{2}$$

Where

$$\operatorname{sgn}(E) = \begin{cases} 1 & for \quad E \geq 0 \\ -1 & for \quad E < 0 \end{cases} \tag{3}$$

and E is the input information. In a joint Fourier processor E is always larger than 0 and hence *sgn (E)* is always 1. The parameters A and μ controls the amount of compression. In the standard systems A=87.6 and μ=255.

Figures 2(A) and 2(B) show the input-output transfer functions of A-law and μ-law encoders defined in equations 1 and 2 respectively. Three different values of A and μ has been selected in order to show the changes in nonlinearity performance of the encoders. The values of A=87.56 and μ= 255 are the standard values used in telecommunication systems.

Figure 3 shows the proposed architecture of A-law/μ-law joint Fourier processor for Adaptive Optics applications. The reference and the signal information correspond to a point source (guide star or multi guide stars[8]) and the object of interest are passing through the distortion medium which produce h + f*h joint image where "h" is the impulse response of the distortion medium, f is the object, "f*h" is the distorted image and asterisk "*" is the convolution symbol. This information is sent to a spatial light modulator and is processed via the joint Fourier processor shown in figure 1.

Theory

In this section we analyze the deconvolution orders using the nonlinear transform method[3]. In the joint Fourier processor shown in figure 3, described in prior section, the joint Fourier transform energy captured by the CCD camera is given by

$$E(\nu_x,\nu_y)=\frac{1}{\lambda f}\left|R(\nu_x,\nu_y)+S(\nu_x,\nu_y)\right|^2 \tag{4}$$

where R is the Fourier transform of the reference information (r), S is the Fourier transform of the signal information (s) and ν_x and ν_y are the spatial frequency coordinates.

Assume an input-output nonlinear transfer function of a processor, *f(E)*, with Fourier transform of *F(ω)* where *E* is the energy and ω is its complement frequency variable. This function can be demonstrated in its summation series format as:

$$f(E)=\sum_{k=0}^{\infty}H_k(\nu_x,\nu_y)\cos\left[2ky_0\nu_y+k(\phi_R-\phi_S)\right] \tag{5}$$

where y_0 is the separation factor between the reference and signal information, Φ_R, Φ_S are the reference and signal phases and $H_k(\nu_x, \nu_y)$ is the weighting factors which is given by

$$H_k(\nu_x,\nu_y)=\frac{\varepsilon_k}{2\pi}i^k\int_{-\infty}^{\infty}F(\omega)\exp\left[i\omega\left(R^2+S^2\right)\right]J_k(2\omega RS)d\omega \tag{6}$$

ε_k is the Neumann factor (ε_k = 1 for k=0 and ε_k=2 for k> 0).

Therefore theoretically as long as the *F(ω),* Fourier transform, of an energy function is known, substituting the *F(ω)* in Eq. 6 would give the correlation[9] or deconvolution weighting orders.

According to Eq. 6, in order to calculate the deconvolution weighting orders of a nonlinear transfer function, the Fourier transform of the input-output nonlinear transfer function is needed. In this section firstly the Fourier transform of the input-output nonlinear transfer function of both μ-law and A-law defined in equations 1 and 2 are calculated.

In order to calculate the Fourier transform of the above functions, it is more convenient to first expand both of these nonlinear transfer functions into their power-law expansion expressions as follows:

$$f(E) = f\left(G_p\right)\left[G_c + 2\sum_{n=1}^{\infty}\frac{1}{2n-1} - 4\sum_{n=1}^{\infty}\frac{S_{Nn}(G_pE)}{2n-1}\right] \tag{7}$$

where G_p is a generic parameter that corresponds to either μ or A and G_c is a generic constant defined as

$$G_c = \begin{cases} 0 \;\; for \;\; \mu - law \\ 1 \;\; for \;\; A - law \end{cases} \tag{8}$$

$f(G_p)$ is a generic constant which is given by:

$$f(G_p) = \begin{cases} f(\mu) = \dfrac{1}{\ln(1+\mu)} \;\; for \;\; the \;\; \mu - law \;\; encoder \\ f(A) = \dfrac{1}{1+\ln A} \;\; for \;\; the \;\; A - law \;\; encoder \end{cases} \tag{9}$$

S_{Nn} is the generic negative nonlinear saturation function defined as:

$$S_{NG_pn}(G_pE) = 1 - \left[S_{PG_p}(G_pE)\right]^n \tag{10}$$

Where $S_{PGp}(G_pE)$ is a positive nonlinear saturation function which is defined for the μ-law and A-law encoders respectively as:

$$S_{PG_p}(G_pE) = \begin{cases} S_{P\mu}(\mu E) = \dfrac{\mu E}{2+\mu E} \;\; for \;\; the \;\; \mu - law \;\; encoder \\ S_{PA}(AE) = \dfrac{AE-1}{AE+1} \;\; for \;\; the \;\; A - law \;\; encoder \end{cases} \tag{11}$$

Each order of the negative saturation function can be fractionally expanded to its first order expansion as:

$$S_{NG_p(2n+1)}(G_pE) = \lim_{\varepsilon\to 0}\sum_{-n}^{+n}\frac{a_{G_pn}}{AE+\gamma+n\varepsilon} \tag{12}$$

Where $\gamma = \begin{cases} 2 & for\ \ the\ \ \mu - law\ \ encoder \\ 1 & for\ \ the\ \ A - law\ \ encoder \end{cases}$ (13)

By combining all equations and knowing the Fourier transform of a negative function as:

$$F(\omega) = -i\,\mathrm{sgn}(\omega)\frac{\pi}{G_p}\exp\left(i\frac{\omega}{G_p}\right)\exp(i\omega E_0), \tag{14}$$

And substituting *F(ω)* in equation 3, the weighting orders for the first and third order of the A-law power-law expansion respectively are:

$$H_{k1}(\nu_x,\nu_y) = \frac{1}{\{(1+AJ_{A-})(1+AJ_{A+})\}^{1/2}}\left(\frac{-2AJ_{A\times}}{1+AJ_{I+}+\{(1+AJ_{A-})(1+AJ_{A+})\}^{1/2}}\right)^k \tag{15}$$

$$\begin{aligned} H_{k3}(\nu_x,\nu_y) &= H_{k1}(\nu_x,\nu_y)\times \\ &\left[\begin{array}{l} 2+3A\left(\frac{J_{A-}}{1+AJ_{A-}}+\frac{J_{A+}}{1+AJ_{A+}}\right)+\frac{3kH_{01}(\nu_x,\nu_y)}{H_{11}(\nu_x,\nu_y)}\left[2+\sqrt{\frac{1+AJ_{A+}}{1+AJ_{A-}}}+\sqrt{\frac{1+AJ_{A-}}{1+AJ_{A+}}}\right]+A^2J_{A+}J_{A-}H^2{}_{01}(\nu_x,\nu_y) \\ +\frac{kH_{01}^2(\nu_x,\nu_y)}{H_{11}(\nu_x,\nu_y)}\left(1+A\left(\frac{J_{A-}}{1+AJ_{A-}}+\frac{J_{A+}}{1+AJ_{A+}}\right)\left(2+\sqrt{\frac{1+AJ_{A+}}{1+AJ_{A-}}}+\sqrt{\frac{1+AJ_{A-}}{1+AJ_{A+}}}\right)\frac{1}{H_{01}(\nu_x,\nu_y)}\right) \end{array}\right] \end{aligned} \tag{16}$$

And the weighting factors for the first and third order of the μ-law power-law expansion respectively are:

$$H_{k1}(\nu_x,\nu_y) = \frac{2}{\{(2+\mu J_{A-})(2+\mu J_{A+})\}^{1/2}}\left(\frac{-2\mu J_{A\times}}{2+\mu J_{I+}+\sqrt{(2+\mu J_{A-})(2+\mu J_{A+})}}\right)^k \tag{17}$$

$$\begin{aligned} H_{k3}(\nu_x,\nu_y) &= H_{k1}(\nu_x,\nu_y)\times \\ &\left[\begin{array}{l} 5+3\mu\left(\frac{J_{A-}}{(2+\mu J_{A-})}+\frac{J_{A+}}{(2+\mu J_{A+})}\right)-\frac{6kH_{01}(\nu_x,\nu_y)}{H_{11}(\nu_x,\nu_y)}\left(2+\sqrt{\frac{2+\mu J_{A-}}{2+\mu J_{A+}}}+\sqrt{\frac{2+\mu J_{A+}}{2+\mu J_{A-}}}\right)+\mu^2J_{A+}J_{A-}H^2{}_{01}(\nu_x,\nu_y) \\ -\frac{kH_{01}^2(\nu_x,\nu_y)}{H_{11}(\nu_x,\nu_y)}\left(1+\mu\left(\frac{J_{A-}}{2+\mu J_{A-}}+\frac{J_{A+}}{2+\mu J_{A+}}\right)\left(2+\sqrt{\frac{2+\mu J_{A+}}{2+\mu J_{A-}}}+\sqrt{\frac{2+\mu J_{A-}}{2+\mu J_{A+}}}\right)\frac{1}{H_{01}(\nu_x,\nu_y)}\right) \end{array}\right] \end{aligned} \tag{18}$$

Where

$$\begin{aligned} J_{A-} &= (R-S)^2 \\ J_{A+} &= (R+S)^2 \\ J_{A\times} &= RS \\ J_{I+} &= R^2+S^2 \end{aligned} \tag{19}$$

Therefore having known each order's weighting factors and combining all together, we can calculate the total weighting factors for both A-law and μ-law encoders as:

$$H_k(\nu_x,\nu_y)=f(G_p)\left[G_c+2\sum_{n=1}^{\infty}\frac{1}{2n-1}-4\sum_{n=1}^{\infty}\frac{1}{2n-1}H_{k(2n-1)}(\nu_x,\nu_y)\right] \quad (20)$$

where G_c=1 for A-law and G_c=0 for μ-law. Substituting equation 20 in equation 5 would show the conversion of the A-law and μ-law input-output transfer functions defined in equations 1 and 2 into a summation series as follow:

$$f(E)=\sum_{k=0}^{\infty}f(G_p)\left[G_c+2\sum_{n=1}^{\infty}\frac{1}{2n-1}-4\sum_{n=1}^{\infty}\frac{1}{2n-1}H_{k(2n-1)}(\nu_x,\nu_y)\right]\cos\left[2ky_0\nu_y+k(\phi_R-\phi_S)\right] \quad (21)$$

For more details on calculating the above equations, see the Appendix.

In order to generate the gray level recovered image, the above equation should be multiplied to a statistical average (generic) filter, $F_s(\nu_x, \nu_y)$[7]. The A-law and μ-law joint Fourier processor can be used either for correlation and convolution, or other signal processing functionalities. Before going further in the simulation, the order expansion in equation 21 used for correlation and convolution is discussed. In the correlation joint Fourier processor, the signal is expected to include the reference matching template, other non-matching signals, clutter and noise[8]. For the most simple case, where the reference and signal information are the same, $\Phi_R = \Phi_S$, *f (E)* simply consists of a sinusoidal grating with periods of $2ky_0$, where k is the grating period. The Fourier transform of equation 21 consists of a periodic delta function convolved with the orders expansion producing the appropriate results for the correlation processing functionality, while for the convolution processing discussed below, only the first order expansion is suitable to perform the functionality. Assume that the signal Fourier spectra is *HF* and the distortion Fourier transform is H. In the deconvolution before the compression that happens in CCD camera two terms of *HFH** and *H*F*H* are produced. These terms after Dynamic Range Compression

produce several orders in equation 20. The signal phase $\Phi_S = \Phi_H + \Phi_F$ and the reference phase is $\Phi_R = \Phi_H$. For image restoration, the k $(\Phi_R - \Phi_S) = \pm k\Phi_F$. This condition is satisfied only for the first order. The other orders have phases of $\pm k\Phi_F$, which produce high order deconvolution terms of the restored image convolved with coefficients. The higher orders can clutter the restored images therefore it is important to know the energy contribution of these orders compare to the first order.

Figure 4 shows plots for the first three order joint spectra coefficient (A) for A-law (B) for the μ-law. The dashed line is for k=1, the dotted line is for k=2 and the dashed dotted line is for k=3.

For small A, the weighting coefficient value is higher for lower orders. This is evident from the plots, at $A=10^{-3}$ the first order coefficient value is 2.086 while the second and the third orders are 0.62. The reason for having the first order higher than the others at small values of A is that the A-law joint Fourier processor is almost linear for small A's (see the figure 3(A), f(E) as a function E). Therefore at small A values the A-law joint Fourier processor functions as a conventional processor (described in chapter 1) and does not introduce higher orders.

As the A value increases, the second order increases to higher values than the third order. All the coefficient are maximized at the same value of A= 0.371. After the maximum point up to almost A=3, as A increases the coefficient values decrease. After the plots intersection, the third order starts increasing to the higher values than the first and second orders while the second order remains the intermediate and the first order becomes the lowest.

At A=87.6, the first, the second and the third orders values are 1.199, 1.6 and 1.97 respectively. This yields that the signal to clutter ratio results from high orders interference could be as low as 0.2232. Therefore enough separation between the reference and the signal information is essential in order to designate separate areas for the orders contributions.

The μ-law coefficients plots illustrated in figure 4(B), showed both similarity and dissimilarities to the A-law coefficients. The μ-law plots show similar results as the A-law's plots where for small A's, the first order had the larger value than the second and the third.

Similar to the A-law plots, the second order coefficients became larger than the third order in the range between $\mu=10^{-2}$ and 2. In contrast to the A-law plots where the coefficients take their maximum values, the μ-law coefficients drop continuously. Similar to the A-law where all coefficients intersected at some A value, the μ-law coefficients also intersect almost at μ=5. Similar to the A-law plots, after the intersection, the third order starts increasing to the higher values than the first and second orders, the second order remains the intermediate and the first order becomes the lowest.

The μ-law has similar behavior as the A-law: for small μ the joint Fourier processor, shown in figure 3(B), is almost linear (f(E) as a function E) and hence at small μ values the μ-law joint Fourier processor is a conventional processor and does not introduce higher orders.

Similar to the A-law at the standard value of μ =255, the first, the second and the third orders values are 2.268, 3.743 and 5.053 respectively. This yields that the signal to clutter ratio results from high orders interference could be as low as 0.1301. Therefore for the μ-law also enough separation between the reference and the signal information is essential in order to designate separate areas for the orders contributions.

The similarities and dissimilarities in the coefficients plots of the μ-law and A-law are attributed to the similarities and dissimilarities in the negative saturation nonlinearity of the A-law and the μ-law used in the analysis. Comparing the negative saturation nonlinearity of the A-law with the negative saturation nonlinearity of the μ-law shows that both the numerators are similar, except

the μ-law numerator has extra nonlinear term. This comparison can be clearer from these equations plots shown in figures 5(A) and 5(B) for A-law and μ-law respectively.

Figure 5(A) shows a secondary maximum for the A-law negative saturation nonlinearity around $AE(v_x,v_y)=1.5$ which could be the reason for having maximum values for the A-law coefficients (figure 4(A)). While for the μ-law shown in figure 5(B) the negative saturation nonlinearity drops continuously and hence there is no maximum value for the μ-law coefficients as it was illustrated in figure 4(B).

The similarities and dissimilarities in the coefficients plots of the A-law and μ-law from their negative saturation nonlinearity functions point of view were discussed. However the A-law coefficients plots for $A\geq 1$ values (Fig. 4(A)) with the μ-law coefficients plots (Fig. 4(B)), can be considered very similar. This can be explained from the A-law and μ-law input-output nonlinear transfer functions plots shown in figure 3 that their functionalities are almost the same for $A\geq 1$ and $\mu\geq 0$ values.

Computer Simulation

Two forms of computer simulation were conducted: direct and indirect. In the direct simulation both of the noisy blurred information and the aberration impulse response were set in a zero array with a separation of almost 256 pixels from their centers. Both were joint Fourier transformed, squared and nonlinearly filtered. In the indirect deconvolution simulation only the first order expansion (k=1) from equation 21 was used. Other orders are irrelevant to be used for deconvolution purposes however for correlation application these orders can be used. Each of these simulations represents different view of the system performance. None represent what exactly could be the case in an optical system.

In direct simulation, contributions of all orders can lead to orders aliasing; while only the first deconvolution order is needed to simulate the deconvolution through an optical system. Aliasing is a simulation artifact and is not applicable in optical systems; in particular aliasing from high orders which interfere with the output result.

In indirect simulation, both the high orders aliasing and interference contributions are removed. Since the aliasing is a simulation artifact, it can be removed however the high orders interference exists in optical systems. Therefore, none of these forms of simulations predicts the exact optical system results. However the combination of direct and indirect simulations should illustrate a good prediction for the deconvolution results.

In the direct simulation a joint image of a 2 x 2 pixels point source and a 128x128 pixels Lena face were located in a 1024 x 1024 zeros (null) array while they are separated by 256 pixels center-to-center. The joint input is convolved with an aberration function to generate the joint blurred image and the blur impulse response. The noise is created by a random-number generator, which produces white Gaussian noise with zero mean and a variance of 1 and is added to the blurred image. Figure 6 shows the simulation results for motion aberration. The motion impulse response was a 2 x 50 pixels rectangle. Figure 6(A) is the joint image of motion impulse response and the noisy blurred image with signal to noise ratio 5, 6(A') is the gray level recovered image using the A-law deconvolution for A=87.6 and 6(A") is the gray level recovered image using the μ-law deconvolution for μ=255. The B and C rows are the same sequence as the A row except for signal to noise ratios 1 and 0.1 respectively.

Figures 7, 8 and 9 are all the same sequence as the figure 6 except for different aberration functions the atmospheric turbulence, misfocusing and phase respectively.

The atmospheric turbulence was defined in reference 10 as $H(\nu_x,\nu_y)=e^{-\beta(\nu_x{}^2+\nu_y{}^2)^{5/6}}$ (22)

where β=0.0025. The misfocusing impulse response was considered as a circle with a diameter of 20 pixels of ones. The phase aberration impulse response was a uniformly distributed random phase-only function of 128 x 128 pixels.

The capability of the proposed system in image recovery without high orders interference was also simulated using equations 15-18 substituted in equation 20. In the direct simulation the same 128 x 128 pixels Lena face is located in a 512 x 512 zeros (null) array as an input image. This input is blurred using the same blur functions described in indirect simulation. The same noise function also was added to the blurred image.

Figures (10, 10'), (11, 11'), (12, 12') and (13, 13') show the simulation results based on the first order nonlinear transform method expansion presented in equation 20.

The non-primed figures represent the results of deconvolution for the following blur functions respectively: motion, atmospheric, misfocusing and phase. For all non-primed figures (A) is the noisy blurred input with SNR= 5, (A') and (A") are the corresponding recovered images via the A-law and the μ-law decovolutions respectively. The B and C rows are sequentially the same as the A row for SNR=1 and SNR=0.1 respectively.

The primed figures represent comparative study of the A-law and μ-law deconvolution with both of the Wiener and the Inverse filters. In all of these figures (A) represents the recovered image via the A-law deconvolution for SNR=1 (the (B') images in the non-primed figures), (B) is the recovered image using Wiener filter, with the expected value of F, (C) is the recovered image using Inverse filtering and (D) is the recovered image using Wiener filter, with the exact value of F. As it is evident in C's figures (primed figures), the Inverse filter was incapable of either recovering or even detecting the image. In these results noise is simply covering the whole array.

By comparing the A's with the D's, it is clear that for all the blur functions tested here the image recovery of noisy blurred signal with SNR=1 via the A-law deconvolution was always better (with a generic shape of the low pass filter or the expected value of F) than the Wiener filter with the exact value of F. When the exact value of F was replaced by a generic shape of the low pass filter or the expected value of F like what it was used in the A-law results, the Wiener filter failed as it is evident in B for all the primed figures.

Both the A-law and the μ-law deconvolutions results showed the possibility of recovering the noisy blurred image for all common forms of blur functions tested here with SNR as low as 0.1. They are associated with noise conversion from low frequencies to high frequencies. This frequency conversion leads for further enhancement of the signal to noise ratio through spreading the noise over the entire array. While in image recovery via the Wiener filter, the noise remains nearly concentrated on the original noisy image area.

Conclusion

This paper introduced for the first time the dynamic range compression deconvolution. Here the dynamic range compression deconvolution implementation via both the A-law and the μ-law encoders (used in telecommunication systems) was proposed. In this approach: (a) the phase information was restored via the combination of the square receiving with the dynamic range compression and (b) the amplitude information (gray level image) was restored through using lowpass filtering.

The dynamic range compression simultaneously enhanced the signal to noise ratio as well as the higher frequencies relative to the lower frequencies which leads to increase noise frequencies. The deconvolution theory of both encoders were developed using the nonlinear transfer method.

The simulation results showed better performance of A-law than the μ-law. Both A-law and μ-law outperformed the Wiener and the Inverse filters.

The A-law and the μ-law encoders are used in both digital and analog systems. The dynamic range compression severity is controlled via the compression parameters A and μ for A-law and the μ-law respectively. The simulation results were improved when these parameters increased.

References

(1) http://hyperphysics.phy-astr.gsu.edu/hbase/audio/tape4.html#c2

(2) John G. Proakis, Masoud Salehi, "Communication Systems Engineering," Prentice Hall (2002)

(3) W. B. Davenport and W. L. Root, "An Introduction to the Theory of Random Signal and Noise," ch. 12-13, p. 255-311, McGraw-Hill, New York (1958)

(4) Rafael C. Gonzalez, Richard E. Woods, "Digital Image Processing," Prentice Hall (2002)

(5) H. Kato and J. W. Goodman, Opt. Commum. 8, 378-381 (1973)

(6) J. L. Horner, "Optical Signal Processing", Academic Press Inc., London (1987)

(7) Bahareh Haji-saeed, "Development of Novel Device Assemblies and Techniques for Improving Adaptive Optics Imaging Systems", PhD. Thesis Dissertation, University of Massachusetts at Lowell (2006)

(8) http://www.ctio.noao.edu/%7Eatokovin/tutorial/intro.html

(9) George Asimellis, J. Khoury, and Charles L. Woods "The effect of saturation nonlinearities in the incoherent to coherent nonlinear joint transform correlator," Journal of the Optical Society of America A, Vol. 13 (1996)

(10) R. E. Hufnagel and N. R. Stanley, "Modulation Transfer Function Associated with Image Transmission through Turbulent Media", J. Opt. Soc. Am., Vol. 54, 52-61(1964)

APPENDIX

The Input-Output nonlinear transfer function of the A-law encoder is

$$g(x) = \frac{1 + \ln(A|x|)}{1 + \ln(A)} \tag{A1}$$

where in joint transform processor, x corresponds to

$$E(\nu_x, \nu_y) = \left| R(\nu_x, \nu_y) + S(\nu_x, \nu_y) \right|^2 \tag{A2}$$

R is the Fourier transform of the reference information and S is the Fourier transform of the signal information. Accordingly equation A1 can be rewritten as

$$g(E) = \frac{1 + \ln(AE(\nu_x, \nu_y))}{1 + \ln(A)} \tag{A3}$$

The nonlinear transfer function of A-law encoder can be expanded into summation of power-law saturation functions

$$g(E) = g(A)\left[1 + 2\left(S_{PA}(AE(\nu_x, \nu_y)) + \frac{1}{3}\left(S_{PA}(AE(\nu_x, \nu_y))\right)^3 + \frac{1}{5}\left(S_{PA}(AE(\nu_x, \nu_y))\right)^5 + \cdots \right)\right] \tag{A4}$$

Where $g(A) = \frac{1}{1 + \ln A}$ (A4.1) and $S_{PA}(AE(\nu_x, \nu_y)) = \frac{AE(\nu_x, \nu_y) - 1}{AE(\nu_x, \nu_y) + 1}$ (A4.2)

S denoted for saturation, P denotes for positive saturation functionality and A is for A-law.

Alternatively the above expansions via positive saturation nonlinearity can be replaced by expansions that consist of negative saturation nonlinearity $S_{NA}(AE)$:

$$g(E) = g(A)\left[1 + 2\sum_{n=1}^{\infty} \frac{1}{2n-1} - 2\sum_{n=1}^{\infty} \frac{S_{NAn}(AE(\nu_x, \nu_y))}{2n-1}\right] \tag{A5}$$

where the *nth* order of negative saturation nonlinearity is defined as:

$$S_{NAn}(AE(\nu_x, \nu_y)) = 1 - \left[S_{PA}(AE(\nu_x, \nu_y))\right]^n \tag{A6}$$

The first three terms of the negative saturation nonlinearities are

$$S_{NA1}(AE) = \frac{2}{AE(\nu_x, \nu_y) + 1} \tag{A7}$$

$$S_{NA3}(AE) = 2\left(\frac{3\left(AE(\nu_x, \nu_y)\right)^2 + 1}{\left(AE(\nu_x, \nu_y) + 1\right)^3} \right) \tag{A8}$$

$$S_{NA5}(AE) = 2\left(\frac{5\left(AE(\nu_x, \nu_y)\right)^4 + 10\left(AE(\nu_x, \nu_y)\right)^2 + 1}{\left(AE(\nu_x, \nu_y) + 1\right)^5} \right) \tag{A9}$$

In the most general form each of the negative nonlinear saturation functions can be expanded into the following form:

$$S_{NA(2n+1)}(AE) = \lim_{\varepsilon \to 0} \sum_{-n}^{n} \frac{a_{An}}{AE + 1 + n\varepsilon} \tag{A10}$$

For example the third order power-law saturation functions it can be expanded in the following form:

$$S_{NA3}(AE) = \frac{3(AE)^2 + 1}{(AE + 1)^3} = \lim_{\varepsilon \to 0} \frac{3x^2 + 1}{(x + 1 - \varepsilon)(x + 1)(x + 1 + \varepsilon)} = \lim_{\varepsilon \to 0} \left[\frac{a_{A_{-1}}}{x + 1 - \varepsilon} + \frac{a_{A_0}}{x + 1} + \frac{a_{A_{+1}}}{x + 1 + \varepsilon} \right] \tag{A11}$$

Where

$$x = AE \tag{A11.1}$$

$$a_{A_{-1}} = \frac{3}{2} - \frac{3}{\varepsilon} + \frac{2}{\varepsilon^2} \tag{A11.2}$$

$$a_{A_0} = -\frac{4}{\varepsilon^2} \tag{A11.3}$$

$$a_{A_{+1}} = \frac{3}{2} + \frac{3}{\varepsilon} + \frac{2}{\varepsilon^2} \tag{A11.4}$$

Similarly for μ-law, the most general form each of the negative nonlinear saturation functions can be expanded into the following form:

$$S_{N\mu(2n+1)}(AE) = \lim_{\varepsilon\to 0}\sum_{-n}^{+n}\frac{a_{\mu n}}{AE+1+n\varepsilon} \tag{A12}$$

For example the third order power-law saturation functions it can be expanded in the following form:

$$S_{N\mu 3}(AE) = \frac{3(\mu E)^2+6\mu E+4}{(2+\mu E)^3} \cong \lim_{\varepsilon\to 0}\frac{3x^2+6x+4}{(2+x-\varepsilon)(2+x)(2+x+\varepsilon)} = \lim_{\varepsilon\to 0}\left[\frac{a_{\mu_{-1}}}{x+2-\varepsilon}+\frac{a_{\mu_0}}{x+2}+\frac{a_{\mu_1}}{x+2+\varepsilon}\right] \tag{A13}$$

Where

$$x = \mu E \tag{A13.1}$$

$$a_{u_{-1}} = 3-\frac{6}{\varepsilon}+\frac{4}{\varepsilon^2} \tag{A13.2}$$

$$a_{\mu_0} = -\frac{8}{\varepsilon^2} \tag{A13.3}$$

$$a_{\mu_{=1}} = 3+\frac{6}{\varepsilon}+\frac{4}{\varepsilon^2} \tag{A13.4}$$

For the first order negative saturation input-output transfer function:

$$f(E) = \frac{1}{1+G_p(E+E_0)} \qquad \text{(A14),}$$

using the nonlinear transfer method[3], the weighing factor for k_{th}-order is given by

$$H_{Rk}(\nu_x,\nu_y) = \frac{1}{\left\{\left[1+G_p(J_{A-}+E_0)\right]\left[1+G_p(J_{A+}+E_0)\right]\right\}^{1/2}}\left(\frac{-2G_pRS}{1+G_p(J_{1+}+E_0)+\left\{\left[1+G_p(J_{A-}+E_0)\right]\left[1+G_p(J_{A+}+E_0)\right]\right\}^{1/2}}\right)^k \tag{A15}$$

Where $G_{p\ is}$ a generic parameter which could be either the beam ratio *m* in two-beam coupling, the *A* or *μ* in *A-law* or the *μ-law* power-law expansions, and the joint spectra momentum are defined as

$$
\begin{aligned}
J_{A-} &= (R-S)^2 \\
J_{A+} &= (R+S)^2 \\
J_{A\times} &= RS \\
J_{I+} &= R^2 + S^2
\end{aligned}
\tag{A16}
$$

According to the above equation the zero order is

$$
H_{R0}(\nu_x, \nu_y) = \frac{1}{\left\{\left[1 + G_p(J_{A-} + E_0)\right]\left[1 + G_p(J_{A+} + E_0)\right]\right\}^{1/2}} \tag{A17}
$$

H_{R0} (ν_x,ν_y) corresponds to the average rectification efficiency of the joint spectra as a result of processing within a device that have negative saturation nonlinearity. And also the k_{th} order power which corresponds to the order of the coefficient amplitude normalized to the processor amplitude rectification efficiency is defined as

$$
P_{Rk}(\nu_x, \nu_y) = \left(\frac{-2G_p RS}{1 + G_p(J_{I+} + E_0) + \left\{\left[1 + G_p(J_{A-} + E_0)\right]\left[1 + G_p(J_{A+} + E_0)\right]\right\}^{1/2}} \right)^k \tag{A18}
$$

Then equation A15 can be represented in the simplest form as

$$
H_{Rk}(\nu_x, \nu_y) = H_{R0}(\nu_x, \nu_y) P_{Rk}(\nu_x, \nu_y) \tag{A19}
$$

For the small incremental change in the value of A, from A to be $A/(1-\varepsilon)$ where ε is a small number, the H_{R0} (ν_x,ν_y) the rectification efficiency is changed to:

$$
H_{R0}(\nu_x, \nu_y) = \left\{ \left[1 + \frac{A}{1 \pm \varepsilon} J_{A-} \right] \left[1 + \frac{A}{1 \pm \varepsilon} J_{A+} \right] \right\}^{-1/2} \cong \frac{\left[1 \pm \varepsilon I_A + \varepsilon^2 O_A\right]}{\sqrt{(1 + AJ_{A-})(1 + AJ_{A+})}} \tag{A20}
$$

Where I_A and O_A defined as:

$$
I_A = \frac{AJ_{A-}}{2(1 + AJ_{A-})} + \frac{AJ_{A+}}{2(1 + AJ_{A+})} \tag{A20.1}
$$

$$
O_A = \frac{A^2 J_{A+} J_{A-}}{4(1 + AJ_{A-})(1 + AJ_{A+})} \tag{A20.2}
$$

Similarly, the coefficient power (the k_{th} order normalized coefficients) can be approximated as:

$$P_{Rk}(\nu_x,\nu_y,\pm\varepsilon)\cong(P_A)^k\left[1\mp\frac{k\varepsilon}{P_A}\left(1+\frac{1}{2}\cdot\sqrt{\frac{1+AJ_{A-}}{1+AJ_{A+}}}+\frac{1}{2}\cdot\sqrt{\frac{1+AJ_{A+}}{1+AJ_{A-}}}\right)-\frac{k\varepsilon^2}{4P_A\sqrt{(1+AJ_{A-})(1+AJ_{A+})}}\right] \quad \text{(A21)}$$
$$=(P_A)^k\left[1\mp J_A\varepsilon-Q_A\varepsilon^2\right]$$

Where J_A, Q_A and P_A are defined respectively as:

$$J_A=\frac{k}{P_A}\left(1+\frac{1}{2}\cdot\sqrt{\frac{1+AJ_{A-}}{1+AJ_{A+}}}+\frac{1}{2}\cdot\sqrt{\frac{1+AJ_{A+}}{1+AJ_{A-}}}\right) \quad \text{(A21.1)}$$

$$Q_A=\frac{k}{4P_A\sqrt{(1+AJ_{A-})(1+AJ_{A+})}} \quad \text{(A21.2)}$$

$$P_A=\frac{2AJ_{A\times}}{1+AJ_{I+}+\sqrt{(1+AJ_{A+})(1+AJ_{A-})}} \quad \text{(A21.3)}$$

Combining the contribution of both the envelope and normalized convolution orders yields that that the weighted convolution orders as results of incremental change in A to be:

$$H_{Rk}(\nu_x,\nu_y,\pm\varepsilon)=\frac{1}{\sqrt{(1+AJ_{A-})(1+AJ_{A+})}}(1\pm\varepsilon I_A+\varepsilon^2O_A)\left[\frac{-2AJ_{A\times}}{1+AJ_{I+}+\sqrt{(1+AJ_{A+})(1+AJ_{A-})}}\right]^k(1\mp\varepsilon J_A-\varepsilon^2Q_A) \quad \text{(A22)}$$

which can be rewritten in the following form

$$\begin{aligned}H_{Rk}(\nu_x,\nu_y,\pm\varepsilon)&=H_{Rk}(\nu_x,\nu_y,0)(1\pm\varepsilon I_A+\varepsilon^2O_A)(1\mp\varepsilon J_A-\varepsilon^2Q_A)\\&=H_{Rk}(\nu_x,\nu_y,0)\left[1\mp(I_A-J_A)\varepsilon+(O_A-Q_A-J_AI_A)\varepsilon^2\right]\\&=H_{Rk}(\nu_x,\nu_y,0)(1\mp a_1\varepsilon+b_1\varepsilon^2)\end{aligned} \quad \text{(A23)}$$

Where $H_{Rk}(\nu_x, \nu_y, 0)$ is the value of $H_{Rk}(\nu_x, \nu_y, \pm\varepsilon)$ when $\varepsilon=0$, $a_1=I_A-J_A$ and $b_1=O_A-Q_A-J_AI_A$.

It was shown in Eq. A11, the expansion of the third order negative saturation nonlinearity as the following format:

$$S_{NA3}(AE)=\frac{3(AE)^2+1}{(AE+1)^3}=\lim_{\varepsilon\to0}\left[\frac{\frac{3}{2}-\frac{3}{\varepsilon}+\frac{2}{\varepsilon^2}}{AE+1-\varepsilon}+\frac{-\frac{4}{\varepsilon^2}}{AE+1}+\frac{\frac{3}{2}+\frac{3}{\varepsilon}+\frac{2}{\varepsilon^2}}{AE+1+\varepsilon}\right] \quad \text{(A24)}$$

If the contribution of the $H_{Rk}(\nu_x, \nu_y, \pm\varepsilon)$ from Eq. A23 for all the terms is substituted in above fractional expansion, the contribution of the third order negative coefficient is given by:

$$H_{Rk3}(\nu_x,\nu_y,\pm\varepsilon)=H_k(\nu_x,\nu_y,-\varepsilon)\left(\frac{3}{2}-\frac{3}{\varepsilon}+\frac{2}{\varepsilon^2}\right)-\frac{4}{\varepsilon^2}H_k(\nu_x,\nu_y,0)+H_k(\nu_x,\nu_y,+\varepsilon)\left(\frac{3}{2}+\frac{3}{\varepsilon}+\frac{2}{\varepsilon^2}\right) \quad \text{(A25)}$$

Substituting the $H_{Rk}(\nu_x, \nu_y, \pm\varepsilon)$ values from equation A23 yields that

$$\begin{aligned}&\left(\frac{3}{2}-\frac{3}{\varepsilon}+\frac{2}{\varepsilon^2}\right)H_{Rk}(\nu_x,\nu_y,0)\left(1-a_1\varepsilon+b_1\varepsilon^2\right)-\frac{4}{\varepsilon^2}H_{Rk}(\nu_x,\nu_y,0)+\left(\frac{3}{2}+\frac{3}{\varepsilon}+\frac{2}{\varepsilon^2}\right)H_{Rk}(\nu_x,\nu_y,0)\left(1+a_1\varepsilon+b_1\varepsilon^2\right)\\&=H_{Rk}(\nu_x,\nu_y,0)\left[2+6(I_A-J_A)+4(O_A-Q_A-I_AJ_A)\right]\end{aligned} \quad \text{(A26)}$$

Substituting all the parameters within the above equation yields that

$$\begin{aligned}H_{Rk3}(\nu_x,\nu_y)=&\frac{1}{\{(1+AJ_{A-})(1+AJ_{A+})\}^{1/2}}\left(\frac{-2AJ_{A\times}}{1+AJ_{I+}+\{(1+AJ_{A-})(1+AJ_{A+})\}^{1/2}}\right)^k\times\\&\left[2+3A\left(\frac{J_{A-}}{1+AJ_{A-}}+\frac{J_{A+}}{1+AJ_{A+}}\right)-\frac{3k\left(1+AJ_{I+}+\{(1+AJ_{A-})(1+AJ_{A+})\}^{1/2}\right)}{2AJ_{A\times}}\left[2+\sqrt{\frac{1+AJ_{A+}}{1+AJ_{A-}}}+\sqrt{\frac{1+AJ_{A-}}{1+AJ_{A+}}}\right]+\frac{A^2J_{A+}J_{A-}}{(1+AJ_{A-})(1+AJ_{A+})}\right.\\&\left.-\frac{k\left(1+AJ_{I+}+\{(1+AJ_{A-})(1+AJ_{A+})\}^{1/2}\right)}{2AJ_{A\times}\{(1+AJ_{A-})(1+AJ_{A+})\}^{1/2}}\left(1+A\left(\frac{J_{A-}}{1+AJ_{A-}}+\frac{J_{A+}}{1+AJ_{A+}}\right)\left(2+\sqrt{\frac{1+AJ_{A+}}{1+AJ_{A-}}}+\sqrt{\frac{1+AJ_{A-}}{1+AJ_{A+}}}\right)\{(1+AJ_{A-})(1+AJ_{A+})\}^{1/2}\right)\right]\end{aligned} \quad \text{(A27)}$$

Using the relationship in equation F2 the above equation can be simplified to

$$\begin{aligned}&H_{Rk3}(\nu_x,\nu_y)=H_{Rk1}(\nu_x,\nu_y)\times\\&\left[2+3A\left(\frac{J_{A-}}{1+AJ_{A-}}+\frac{J_{A+}}{1+AJ_{A+}}\right)+\frac{3kH_{R01}(\nu_x,\nu_y)}{H_{R11}(\nu_x,\nu_y)}\left[2+\sqrt{\frac{1+AJ_{A+}}{1+AJ_{A-}}}+\sqrt{\frac{1+AJ_{A-}}{1+AJ_{A+}}}\right]+A^2J_{A+}J_{A-}H^2{}_{R01}(\nu_x,\nu_y)\right.\\&\left.+\frac{kH^2_{R01}(\nu_x,\nu_y)}{H_{R11}(\nu_x,\nu_y)}\left(1+A\left(\frac{J_{A-}}{1+AJ_{A-}}+\frac{J_{A+}}{1+AJ_{A+}}\right)\left(2+\sqrt{\frac{1+AJ_{A+}}{1+AJ_{A-}}}+\sqrt{\frac{1+AJ_{A-}}{1+AJ_{A+}}}\right)\frac{1}{H_{R01}(\nu_x,\nu_y)}\right)\right]\end{aligned} \quad \text{(A28)}$$

For the analysis of third and high order power-law negative saturation functionality of the μ-law, the same steps as in the analysis of the A-law was proceeded. The deconvolution orders can be approximated as

$$\begin{aligned}H_{Rk3}(\nu_x,\nu_y)=&\frac{2}{\{(2+\mu J_{A-})(2+\mu J_{A+})\}^{1/2}}\left(\frac{-2\mu J_{A\times}}{2+\mu J_{I+}+\sqrt{(2+\mu J_{A-})(2+\mu J_{A+})}}\right)^k\times\\&\left[5+3\mu\left(\frac{J_{A-}}{(2+\mu J_{A-})}+\frac{J_{A+}}{(2+\mu J_{A+})}\right)-\frac{3k\left(2+\mu J_{I+}+\sqrt{(2+\mu J_{A-})(2+\mu J_{A+})}\right)}{\mu J_{A\times}}\left(2+\sqrt{\frac{2+\mu J_{A-}}{2+\mu J_{A+}}}+\sqrt{\frac{2+\mu J_{A+}}{2+\mu J_{A-}}}\right)\right.\\&\left.+\frac{\mu^2J_{A-}J_{A+}}{(2+\mu J_{A-})(2+\mu J_{A+})}-\frac{k\left(2+\mu J_{I+}+\sqrt{(2+\mu J_{A-})(2+\mu J_{A+})}\right)}{\mu J_{A\times}\sqrt{(2+\mu J_{A-})(2+\mu J_{A+})}}\left(1+\mu\left(\frac{J_{A-}}{2+\mu J_{A-}}+\frac{J_{A+}}{2+\mu J_{A+}}\right)\left(2+\sqrt{\frac{2+\mu J_{A+}}{2+\mu J_{A-}}}+\sqrt{\frac{2+\mu J_{A-}}{2+\mu J_{A+}}}\right)\{(2+\mu J_{A-})(2+\mu J_{A+})\}^{1/2}\right)\right]\end{aligned} \quad \text{(A29)}$$

The Eq. A29 can be simplified to the following format

$$H_{Rk3}(\nu_x,\nu_y)=H_{Rk1}(\nu_x,\nu_y)\times$$
$$\left[\begin{array}{l} 5+3\mu\left(\frac{J_{A-}}{(2+\mu J_{A-})}+\frac{J_{A+}}{(2+\mu J_{A+})}\right)-\frac{6kH_{R01}(\nu_x,\nu_y)}{H_{R11}(\nu_x,\nu_y)}\left(2+\sqrt{\frac{2+\mu J_{A-}}{2+\mu J_{A+}}}+\sqrt{\frac{2+\mu J_{A+}}{2+\mu J_{A-}}}\right)+\mu^2 J_{A+}J_{A-}H^2{}_{R01}(\nu_x,\nu_y) \\ -\frac{kH^2_{R01}(\nu_x,\nu_y)}{H_{R11}(\nu_x,\nu_y)}\left(1+\mu\left(\frac{J_{A-}}{2+\mu J_{A-}}+\frac{J_{A+}}{2+\mu J_{A+}}\right)\left(2+\sqrt{\frac{2+\mu J_{A+}}{2+\mu J_{A-}}}+\sqrt{\frac{2+\mu J_{A-}}{2+\mu J_{A+}}}\right)\frac{1}{H_{R01}(\nu_x,\nu_y)}\right) \end{array}\right] \quad \text{(A30)}$$

Figures Captions:

Figure 1. Joint Fourier processor via A-law/μ-law

Figure 2. (A) A-law input-output transfer function for A=1, 5 and 87. 56, (B) μ-law input-output transfer function μ= 0, 5 and 255

Figure 3. Adaptive Optics imaging system for image restoration using A-law/μ-law

Figure 4. Joint spectra coefficient for (A) A-law and (B) μ-law

Figure 5. Third order negative saturation nonlinearity for (A) A-law and (B) μ-law

Figure 6. Motion aberration simulation results, (A) the joint image of motion impulse response and the noisy blurred image with signal to noise ratio 5, (A') the gray level recovered image using the A-law deconvolution for A=87.6 and (A") the gray level recovered image using the μ-law deconvolution for μ=255. The B and C rows are the same sequence as the A row except for signal to noise ratios 1 and 0.1 respectively.

Figure 7. Atmospheric turbulence simulation results (A) the joint image of motion impulse response and the noisy blurred image with signal to noise ratio 5, (A') the gray level recovered image using the A-law deconvolution for A=87.6 and (A") the gray level recovered image using the μ-law deconvolution for μ=255. The B and C rows are the same sequence as the A row except for signal to noise ratios 1 and 0.1 respectively.

Figure 8. Misfocusing aberration simulation results (A) the joint image of misfocusing impulse response and the noisy blurred image with signal to noise ratio 5, (A') the gray level recovered image using the A-law deconvolution for A=87.6 and (A") the gray level recovered image using the μ-law deconvolution for μ=255. The B and C rows are the same sequence as the A row except for signal to noise ratios 1 and 0.1 respectively.

Figure 9. Phase-only aberration simulation results (A) the joint image of Phase-only impulse response and the noisy blurred image with signal to noise ratio 5, (A') the gray level recovered image using the A-law deconvolution for A=87.6 and (A") the gray level recovered image using the μ-law deconvolution for μ=255. The B and C rows are the same sequence as the A row except for signal to noise ratios 1 and 0.1 respectively.

Figure 10. Motion aberration indirect simulation results (A) the noisy blurred input with SNR= 5, (A') and (A") are the corresponding recovered images via the A-law and the μ-law decovolutions respectively. The B and C rows are sequentially the same as the A row for SNR=1 and SNR=0.1 respectively.

Figure 10'. A-law deconvolution result for the motion aberration compare to Wiener and Inverese filters result (A) the recovered image via the A-law deconvolution for SNR=1, (B) the recovered image using Wiener filter, with the expected value of F, (C) the recovered image using Inverse filtering and (D) is the recovered image using Wiener filter, with the exact value of F

Figure 11. Atmospheric turbulence indirect simulation results (A) the noisy blurred input with SNR= 5, (A') and (A") are the corresponding recovered images via the A-law and the μ-law decovolutions respectively. The B and C rows are sequentially the same as the A row for SNR=1 and SNR=0.1 respectively.

Figure 11'. A-law deconvolution result for the Atmospheric turbulence compare to Wiener and Inverse filters result (A) the recovered image via the A-law deconvolution for SNR=1, (B) the recovered image using Wiener filter, with the expected value of F, (C) the recovered image using Inverse filtering and (D) is the recovered image using Wiener filter, with the exact value of F

Figure 12. Misfocusing aberration indirect simulation results (A) the noisy blurred input with SNR= 5, (A') and (A") are the corresponding recovered images via the A-law and the μ-law

decovolutions respectively. The B and C rows are sequentially the same as the A row for SNR=1 and SNR=0.1 respectively.

Figure 12'. A-law deconvolution result for the Misfocusing aberration compare to Wiener and Inverese filters result (A) the recovered image via the A-law deconvolution for SNR=1, (B) the recovered image using Wiener filter, with the expected value of F, (C) the recovered image using Inverse filtering and (D) is the recovered image using Wiener filter, with the exact value of F

Figure 13. Phase-only aberration indirect simulation results (A) the noisy blurred input with SNR= 5, (A') and (A") are the corresponding recovered images via the A-law and the μ-law decovolutions respectively. The B and C rows are sequentially the same as the A row for SNR=1 and SNR=0.1 respectively.

Figure 13'. A-law deconvolution result for the Phase-only aberration compare to Wiener and Inverse filters result (A) the recovered image via the A-law deconvolution for SNR=1, (B) the recovered image using Wiener filter, with the expected value of F, (C) the recovered image using Inverse filtering and (D) is the recovered image using Wiener filter, with the exact value of F

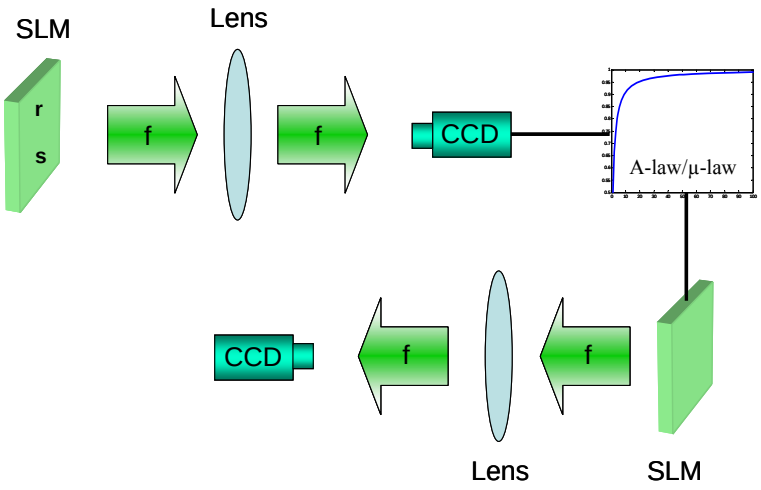

Figure 1

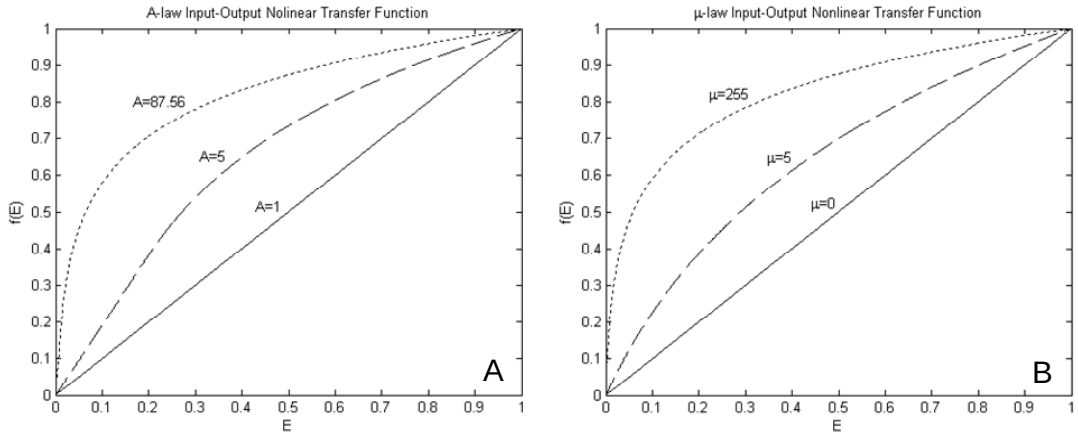

Figure 2

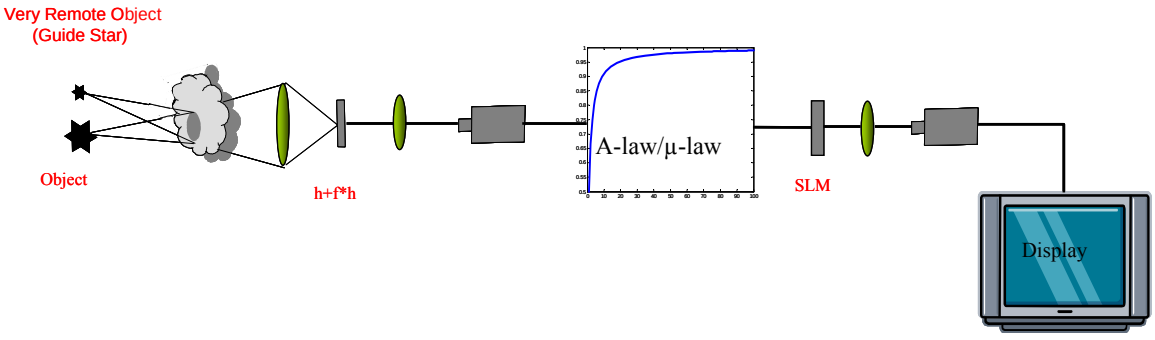

Figure 3

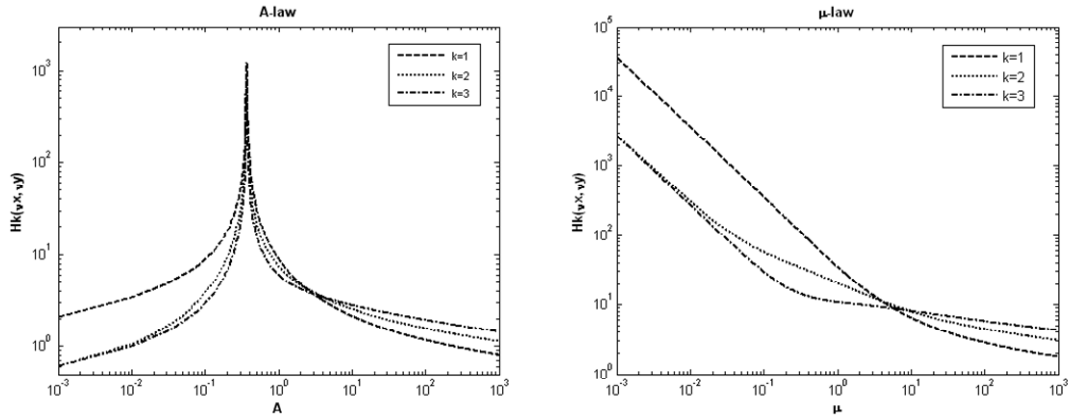

(A) (B)

Figure 4

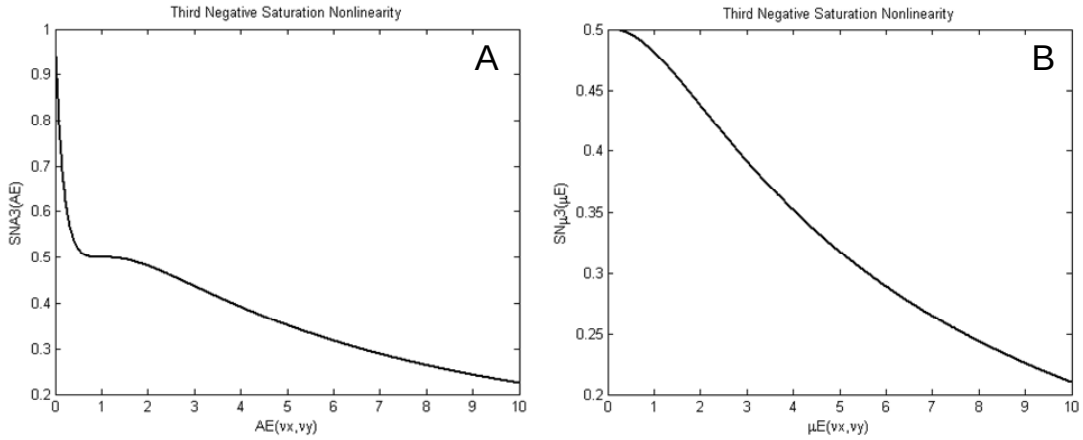

Figure 5

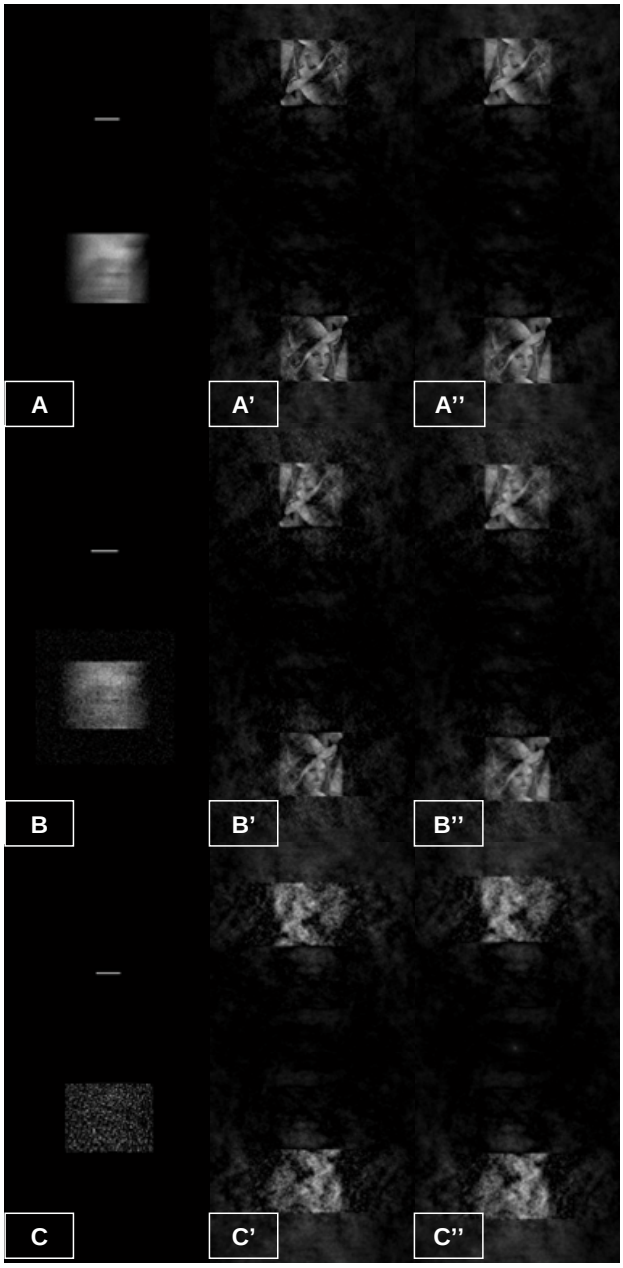

Figure 6

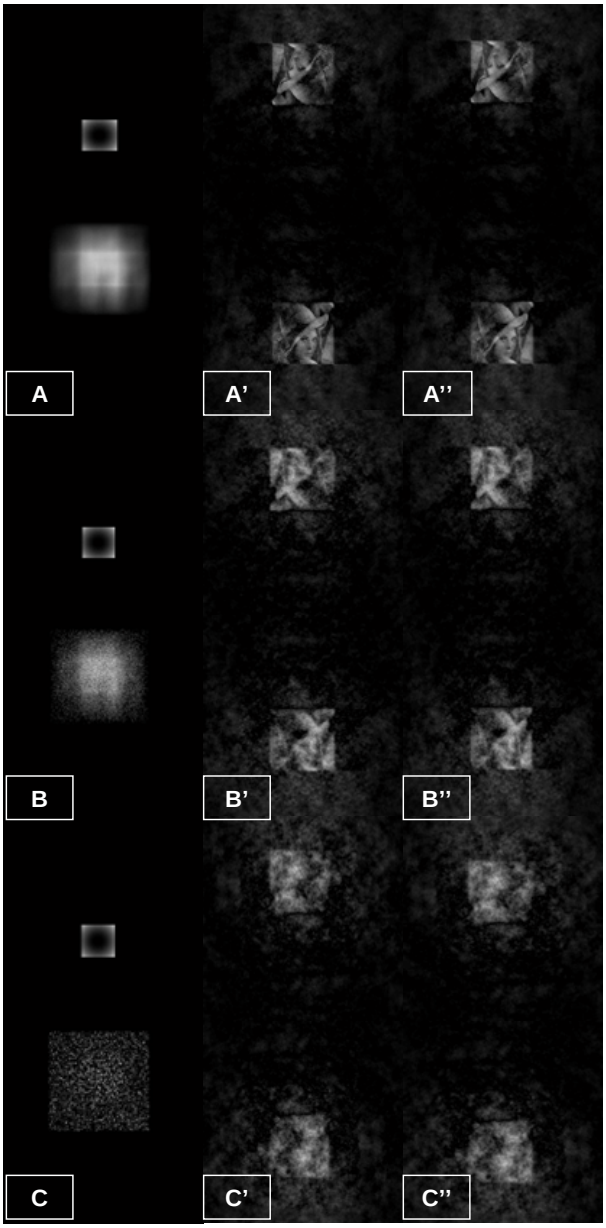

Figure 7

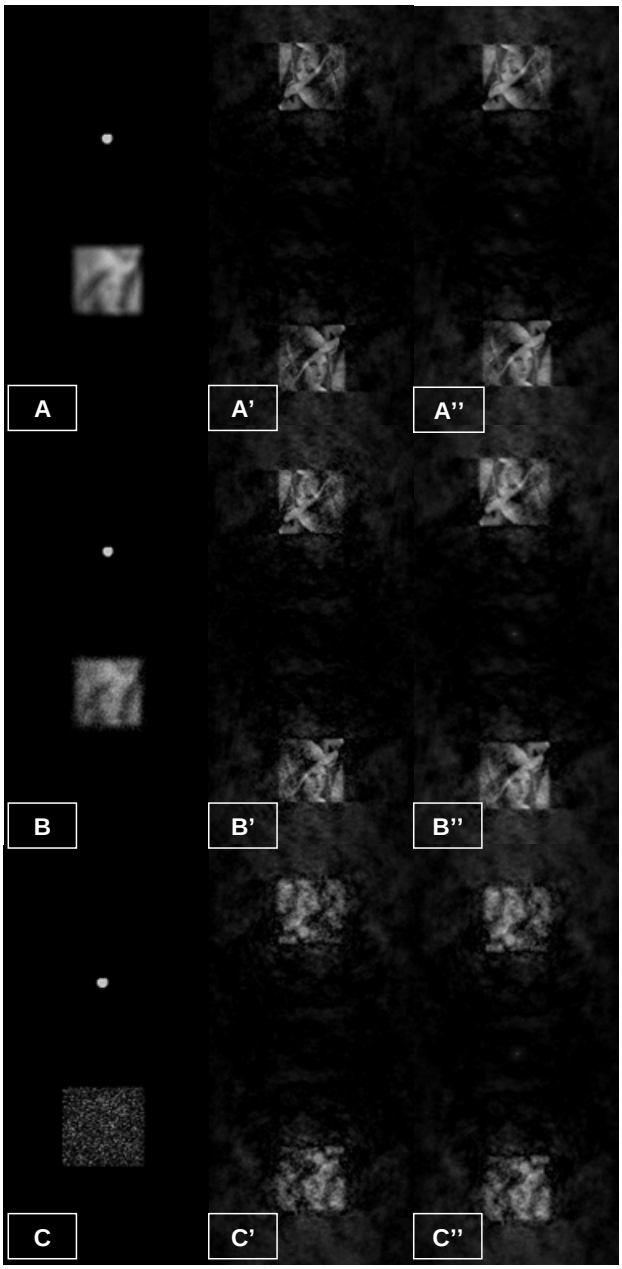

Figure 8

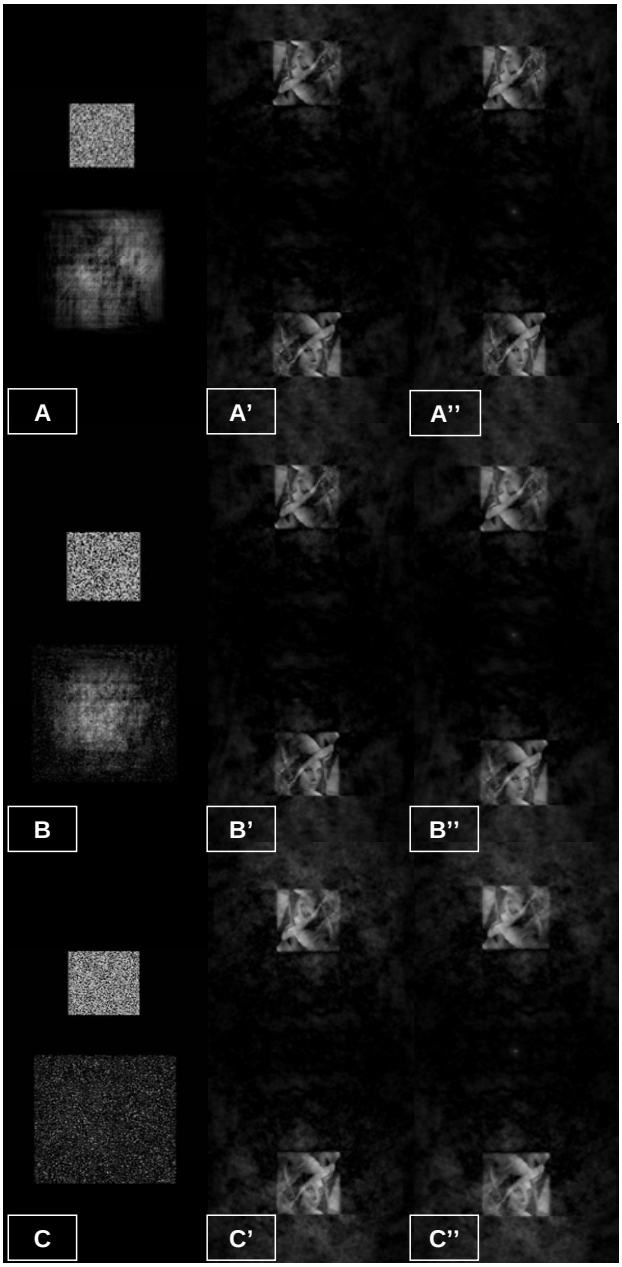

Figure 9

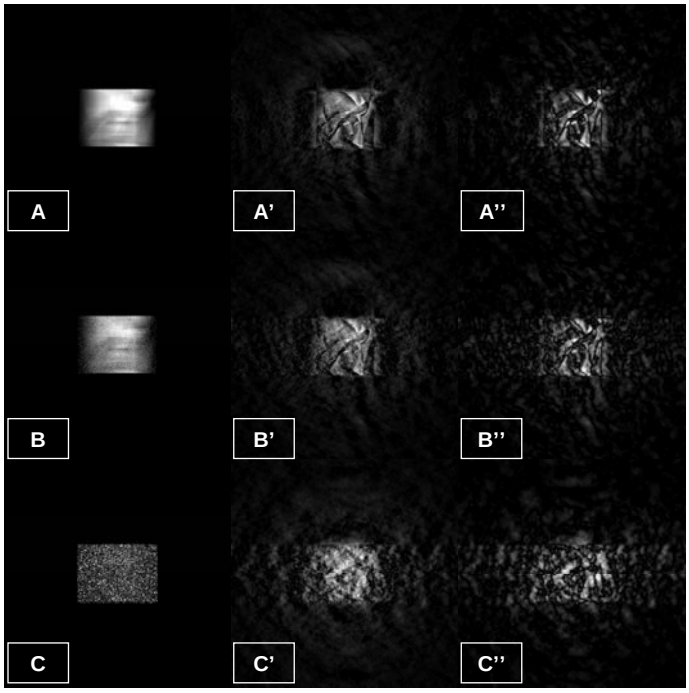

Figure 10

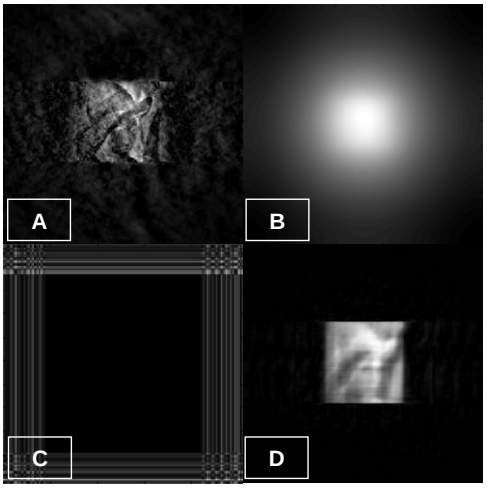

Figure 10'

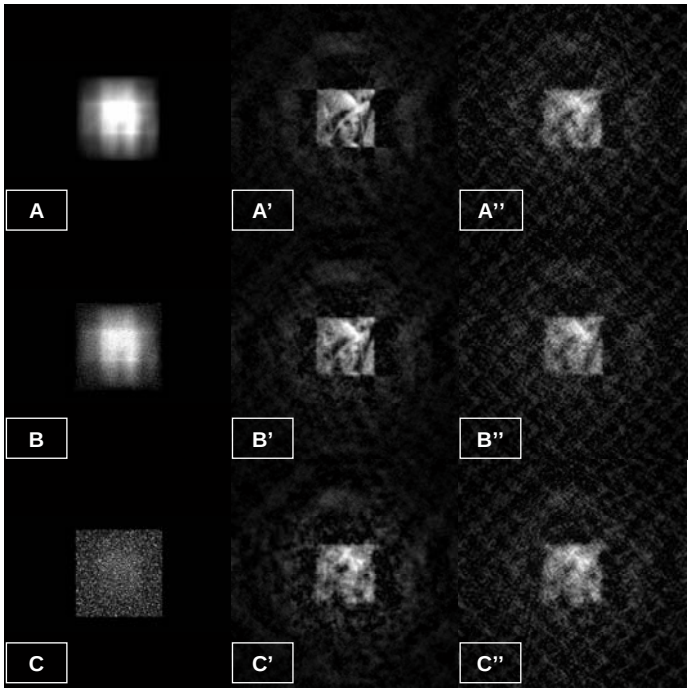

Figure 11

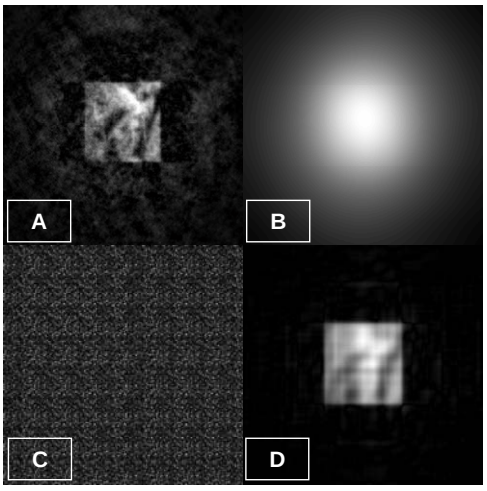

Figure 11'

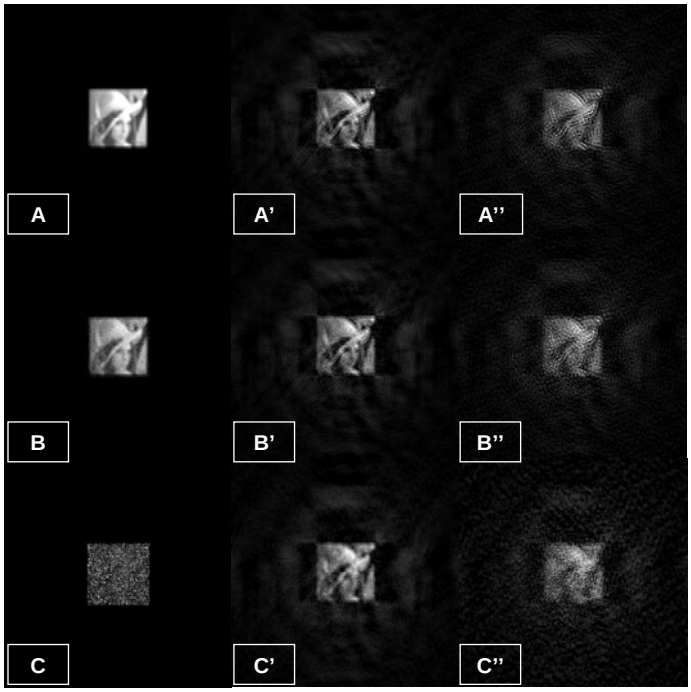

Figure 12

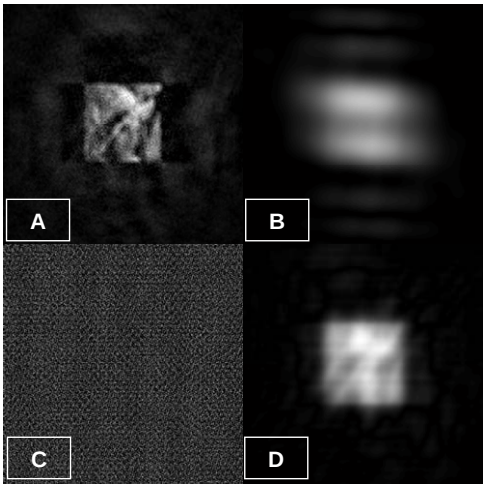

Figure 12'

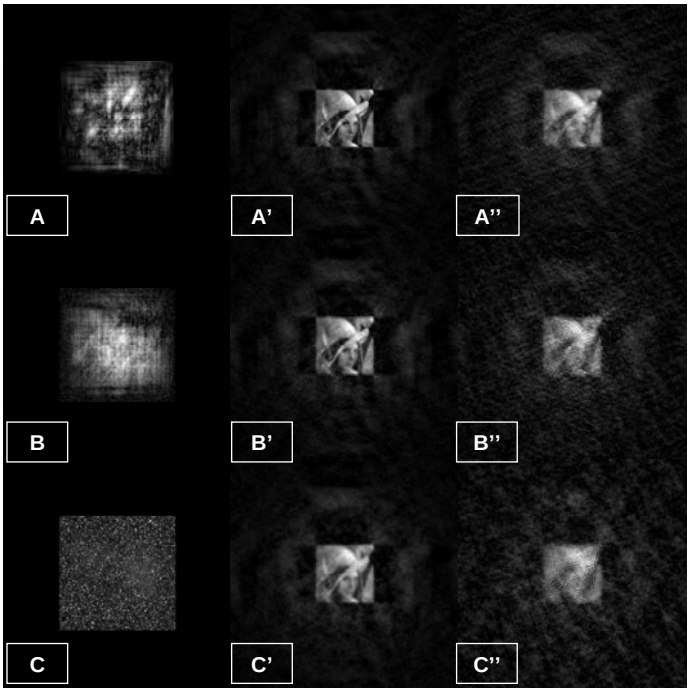

Figure 13

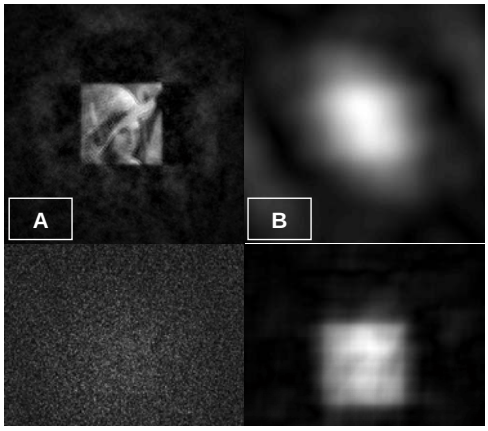

Figure 13'